




Microstructure and mechanical properties of Ti_3AlC_2 reinforced Al–4.5 Cu–1.5 Mg composites fabricated by powder metallurgy

X. N. Li^{1,2}, P. Y. Li², Z. Q. Liu², K. Ma², Z. Y. Liu^{2*} , B. L. Xiao^{2,*}, and Z. Y. Ma²

¹School of Materials Science and Engineering, University of Science and Technology of China, 72 Wenhua Road, Shenyang 110016, China

²Shi-Changxu Innovation Center for Advanced Materials, Institute of Metal Research, Chinese Academy of Science, 72 Wenhua Road, Shenyang 110016, China

Received: 7 December 2022

Accepted: 10 January 2023

Published online:

1 February 2023

© The Author(s), under exclusive licence to Springer Science+Business Media, LLC, part of Springer Nature 2023

ABSTRACT

Ti_3AlC_2 reinforced 2009Al ($Ti_3AlC_2/2009Al$) composites with various Ti_3AlC_2 concentrations were fabricated by high energy ball milling combined with powder metallurgy. Microstructure, phases and mechanical properties of $Ti_3AlC_2/2009Al$ composites were investigated. The results indicate that, only a few and fine reaction product of $AlTi_2$ could be detected, indicating that the interface reaction was effectively controlled. Ti_3AlC_2 extraction and delamination effectively facilitated the compatible deformation between Ti_3AlC_2 and Al matrix. All of these resulted in a much higher strength (688 MPa) and elongation (8.6%) of the $Ti_3AlC_2/2009Al$ composite, as compared with most of the nanoreinforced aluminum matrix composites.

Introduction

Aluminum matrix composites (AMCs) have drawn much attention in the fields of aerospace and automotive industries, due to their high specific strength, high specific modulus and wear resistance [1–3]. In general, the reinforcement, such as SiC [4–6], B_4C [7], Al_2O_3 [8] or TiB_2 [9], could significantly improve the strength and modulus of the AMCs. But the poor

compatible deformation capability between the reinforcement and aluminum matrix dramatically reduced the elongation of the composites, which restricted the application field.

One of the most effective techniques for enhancing the strength–ductility was to introduce ductile phase, which could effectively bridge the crack in the wake of growing crack [10, 11]. Recently, a kind of novel MAX ceramic has received significant attention because of their special performance. This ternary

Handling Editor: Naiqin Zhao.

Address correspondence to E-mail: zyliu@imr.ac.cn; blxiao@imr.ac.cn

layered compound with hexagonal structure, has the general formula of $M_{n+1}AX_n$ ($n = 1, 2, 3$), where M is a transition metal, A is an A-group element, and X is carbon and/or nitrogen [12–14]. In the layered hexagonal crystal structure, the near close-packed layers of M interleaves with layers of pure A-group elements, which make it combine the merits of both metals and ceramics [15].

The unique deformation of MAX ceramic in terms of delamination and the formation of kinking band could also effectively facilitate the compatible deformation between the reinforcement and metal matrix [15, 16]. This indicated that the AMCs reinforced with MAX ceramic could achieve high strength and ductility in theory, comparing with those reinforced by traditional ceramics. However, in most of the previous investigations [15, 16], the majority of MAX ceramics were of several tens of micrometer sized and particle contents were fairly high in MAX ceramic reinforced AMCs. This would increase the number of weak layers between A and $M_{n+1}X_n$ in MAX ceramics, and the strength of MAX ceramic reinforced AMCs was weakened. Thus, most of the previous studies [13, 14, 17–19] could only focus on the compressive and tribological properties of MAX ceramic reinforced AMCs, while the tensile properties have not been reported so far.

Generally, the tensile strength of the AMCs reinforced by particles would increase with reducing the particle size [20]. It is possible to obtain higher strength by reducing the number of interlayers in single MAX particle, for the weak bonding force between the layer of A and $M_{n+1}X_n$, just like graphene [21, 22]. Recently, high energy ball milling (HEBM) has been widely used to fabricate nanomaterials reinforced MMCs by the high shearing stress generated locally due to the severe collision and friction among balls [1, 23–26]. So, it is likely to obtain the MAX particles with less weak interlayer by HEBM, and led to enhanced properties of the AMCs reinforced by MAX.

But the interfacial contact area would increase and the interfacial reaction aggravated as well due to the refinement of MAX particles [13, 18]. Varying reaction products such as Al_3Ti , $TiAl_2$, TiC and Al_4C_3 et al. generated under different fabrication temperature and had a great influence on the compressive strength of MAX/Al composites as reported by previous studies [12, 13, 19, 27–29]. Under the circumstances, the interface structure characteristic, such as

the variety, distribution state, overall dimensions, amount and size of the in-situ phases needed to be strictly controlled. This would significantly complicate the design and fabrication of MAX/Al composites. Therefore, developing the MAX/Al composites with clean interface was necessary. So far, reducing temperature was the most efficient way to inhibit the interface reaction [17, 19, 30–32]. In general, powder metallurgy (PM) method had a much lower temperature, as compared with liquid methods, such as stir casting or infiltration. Thus, PM could be an effect process for fabricating MAX/Al composites.

In this study, Ti_3AlC_2 was chosen as the typical MAX ceramic, and the Ti_3AlC_2 reinforced Al–4.5 Cu–1.5 Mg composites ($Ti_3AlC_2/2009Al$) were fabricated through HEBM combined with PM method. Microstructure and mechanical properties of $Ti_3AlC_2/2009Al$ composites with varying Ti_3AlC_2 concentrations were compared. The aim of this present work was to (a) understand the microstructure of $Ti_3AlC_2/2009Al$ composites; (b) develop the $Ti_3AlC_2/2009Al$ composites with high strength and ductility.

Experimental

Fabrication and mechanical property tests of $Ti_3AlC_2/2009Al$ composites

The raw material of Ti_3AlC_2 powders (Fig. 1a) had an average size of $\sim 38 \mu m$, and the magnified SEM images (Fig. 1b) revealed that the Ti_3AlC_2 particle had an obvious multiple-layer structure. The $Ti_3AlC_2/2009Al$ composites were prepared through HEBM combined with PM method, and the preparation process flow is shown in Fig. 2. Firstly, the Ti_3AlC_2 with various volume fractions (1.5, 2.25, 3 vol.%) were milled with 2009Al powders, respectively, in an attritor for 6 h, and conducted at a rotational speed of 400 RPM with a ball powder ratio of 15:1. Secondly, the milled $Ti_3AlC_2/2009Al$ powders were cold compacted into a cylinder die and degassed. The cold compacted billets were hot pressed at 540 °C for 1.5 h. Then, the as-hot pressed billets were hot extruded at 450 °C with an extrusion ratio of 16:1. Finally, the $Ti_3AlC_2/2009Al$ composites were solid-solution-treated at 500 °C for 2 h, quenched into water at room temperature, and then aged at room temperature for at least 4 days (i.e., T4

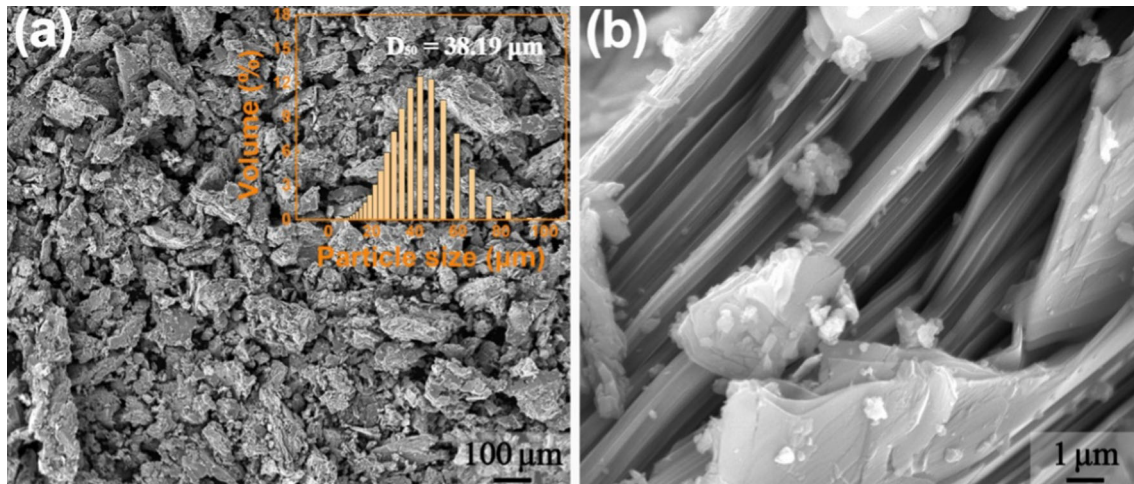


Figure 1 SEM images showing the morphology of the raw Ti_3AlC_2 powders.

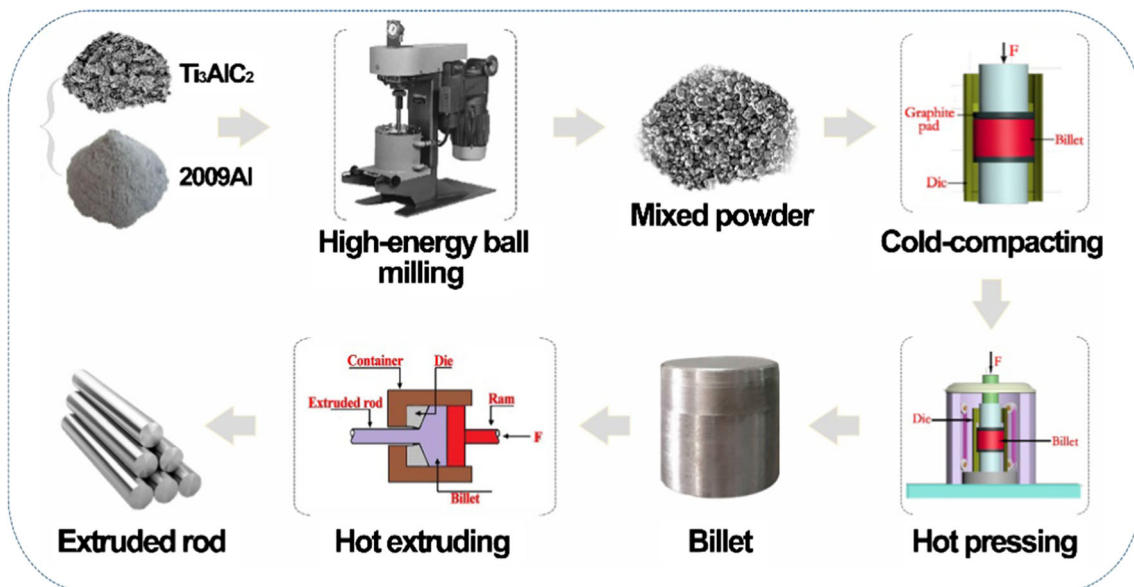


Figure 2 Schematic illustration for the fabrication route of the $\text{Ti}_3\text{AlC}_2/2009\text{Al}$ composites.

treatment). For comparison, 2009Al alloy was also fabricated under the same conditions.

The dog-bone-shaped tensile specimens with nominal dimensions of $2 \times 4 \times 12$ mm were machined from the extruded bars, which kept the tensile axis paralleling to the extrusion direction. The tensile tests were conducted at a strain rate of $1 \times 10^{-3} \text{ s}^{-1}$ on an Instron 5982 universal testing machine, and at least 3 tensile specimens were tested for each composite.

Characterization of the microstructure

The specimens for microstructural examinations were sectioned along the extrusion direction. The phase constituents of the composites were determined by X-ray diffraction (XRD, X'Pert PRO, Holland). Transmission electron microscope (TEM, Tecnai G2 20) with scanning transmission electron microscopy (STEM), energy dispersive spectrometer (EDS), selected area electron diffraction (SAED) and high resolution transmission electron microscopy (HRTEM) at 200 kV was used to examine the phase and detailed microstructure of $\text{Ti}_3\text{AlC}_2/2009\text{Al}$ composites. Scanning electron microscopy (SEM,

Inspect F50) with EDS was used to characterize the phases and fracture surfaces of Ti_3AlC_2 /2009Al composites.

Results and discussions

Microstructure and phase analysis

Figure 3 shows the XRD patterns of the raw Ti_3AlC_2 and Ti_3AlC_2 /2009Al composites with different Ti_3AlC_2 concentrations. It can be clearly seen that only Ti_3AlC_2 (Hexagonal, $P63/mmc$, $a = 3.069 \text{ \AA}$, $c = 18.501 \text{ \AA}$) peaks were observed for the raw Ti_3AlC_2 , and no other impurities such as TiC or Ti_xAl_y intermetallic were observed [13, 17]. Ti_3AlC_2 , CuAl_2 and Al were the dominated phases in Ti_3AlC_2 /2009Al composites, which indicated that the reaction products were effectively controlled. Further, the Al_4C_3 phase was also observed in all Ti_3AlC_2 /2009Al composites, but the intensity of Al_4C_3 peak did not increase with increasing the Ti_3AlC_2 concentrations. This result indicated that the Al_4C_3 phase was generated according to the residue of process control agent rather than interfacial reaction, just as other composites fabricated by HEBM [25, 33–35].

Microstructure of Ti_3AlC_2 /2009Al composites with different Ti_3AlC_2 concentrations is shown in Fig. 4. According to the back-scattered SEM images (Fig. 4a) and corresponding EDS maps of element Ti, C and Cu (Fig. 4b–d) of 2.25 vol.% Ti_3AlC_2 /2009Al composite, it can be seen that the Ti_3AlC_2 particles ($\sim 40 \mu\text{m}$) with large sizes were successfully broken

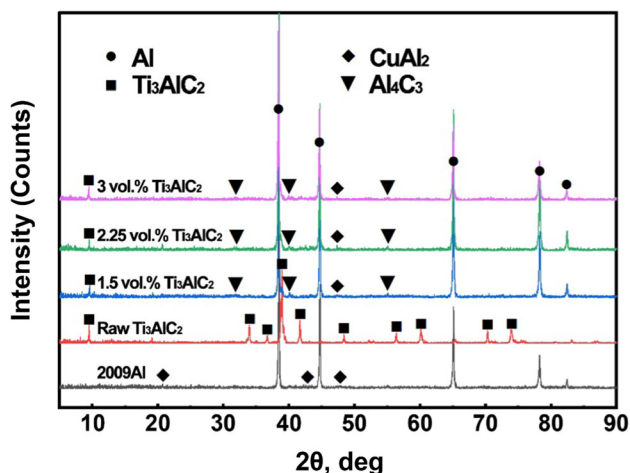


Figure 3 XRD patterns of raw Ti_3AlC_2 and Ti_3AlC_2 /2009Al composites with different Ti_3AlC_2 concentrations.

into small pieces ($\sim 3 \mu\text{m}$ long, $\sim 1 \mu\text{m}$ broad) after HEBM. And this particle size was much smaller than other MAX reinforced MMCs [13, 14, 17, 19, 30]. The weak bonding force between the layer of Al and Ti_3C_2 [15, 16] and severe mechanical effect during HEBM was the dominant reasons.

Back-scattered SEM images of Ti_3AlC_2 /2009Al composites with various Ti_3AlC_2 concentrations are shown in Fig. 4e–h. It can be seen that some ruptured Ti_3AlC_2 could be observed in the 2.25 and 3 vol.% Ti_3AlC_2 /2009Al composites, and the number of particles with cracks in the 3 vol.% Ti_3AlC_2 /2009Al composite was higher than that of 2.25 vol.% Ti_3AlC_2 /2009Al composite. This indicates that the breakage of single Ti_3AlC_2 particle was insufficient when Ti_3AlC_2 concentration increased to 3 vol.%; and thus, the size of Ti_3AlC_2 in 3 vol.% Ti_3AlC_2 /2009Al composite was larger than that of 1.5 vol.% and 2.25 vol.% Ti_3AlC_2 /2009Al composites.

To confirm the phase constitution of the composites exactly, 2.25 vol.% Ti_3AlC_2 /2009Al composite was characterized by TEM. Three obvious phases could be identified under the high angle annular dark field (HAADF) mode, and the three phases were marked with three different colors (Fig. 5a). The EDS (Fig. 5b–e) and SAED (Fig. 5f–h) indicated that the three phases were, respectively, Ti_3AlC_2 , AlTi_2 and $\text{Al}_{6.35}\text{Cu}_{2.4}\text{Fe}_{1.25}$. The $\text{Al}_{6.35}\text{Cu}_{2.4}\text{Fe}_{1.25}$ phase was the impurity phase resulted from the Fe imported during milling, and the negative effect of $\text{Al}_{6.35}\text{Cu}_{2.4}\text{Fe}_{1.25}$ could be weakened for the small size and relatively low content.

It should be mentioned that AlTi_2 phase has not been reported in the previous studies of MAX/Al composites [36–38]. Usually, Al–Ti reaction could form intermetallic compounds such as Al_2Ti_5 , Al_3Ti , AlTi_2 , AlTi_3 and AlTi phases [10, 39]. Among of them, Al_3Ti was usually generated for the lower free energy of formation [17, 18, 28]. But in this work, AlTi_2 was detected rather than Al_3Ti . It is believed that, both of the phases ($\text{Al}_{6.35}\text{Cu}_{2.4}\text{Fe}_{1.25}$ and AlTi_2) are metastable on account of the relatively low sintering temperature with PM technology. As reported by previous studies, the intermetallic compound of AlTi_2 could effectively strengthen the compressive properties of Al matrix composites [10, 11, 39].

Figure 6a shows the bright-field TEM image of Ti_3AlC_2 and aluminum interfacial region of 2.25 vol.% Ti_3AlC_2 /2009Al composite. The HRTEM image of sample was aligned to Al [110] zone axis,

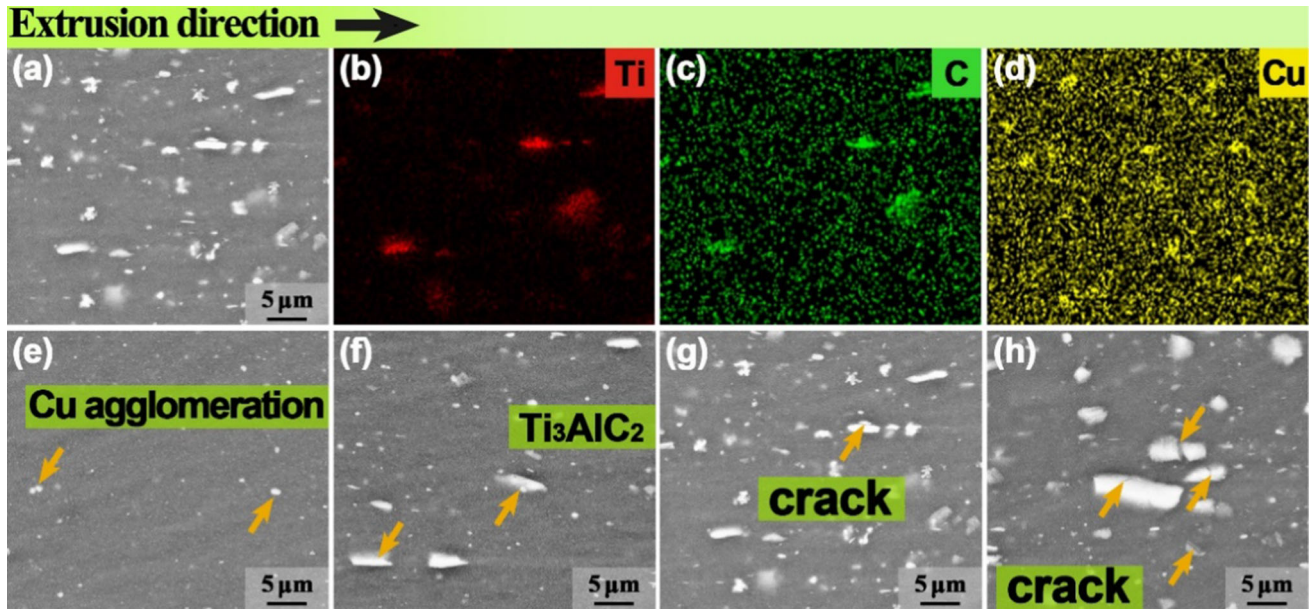


Figure 4 Back-scattered SEM images (a) and corresponding EDS maps of Ti (b), C (c) and Cu (d) of 2.25 vol.% Ti_3AlC_2 /2009Al composite; back-scattered SEM images of Ti_3AlC_2 /2009Al

composites with different Ti_3AlC_2 concentrations: 0 vol.% (e), 1.5 vol.% (f), 2.25 vol.% (g) and 3 vol.% (h).

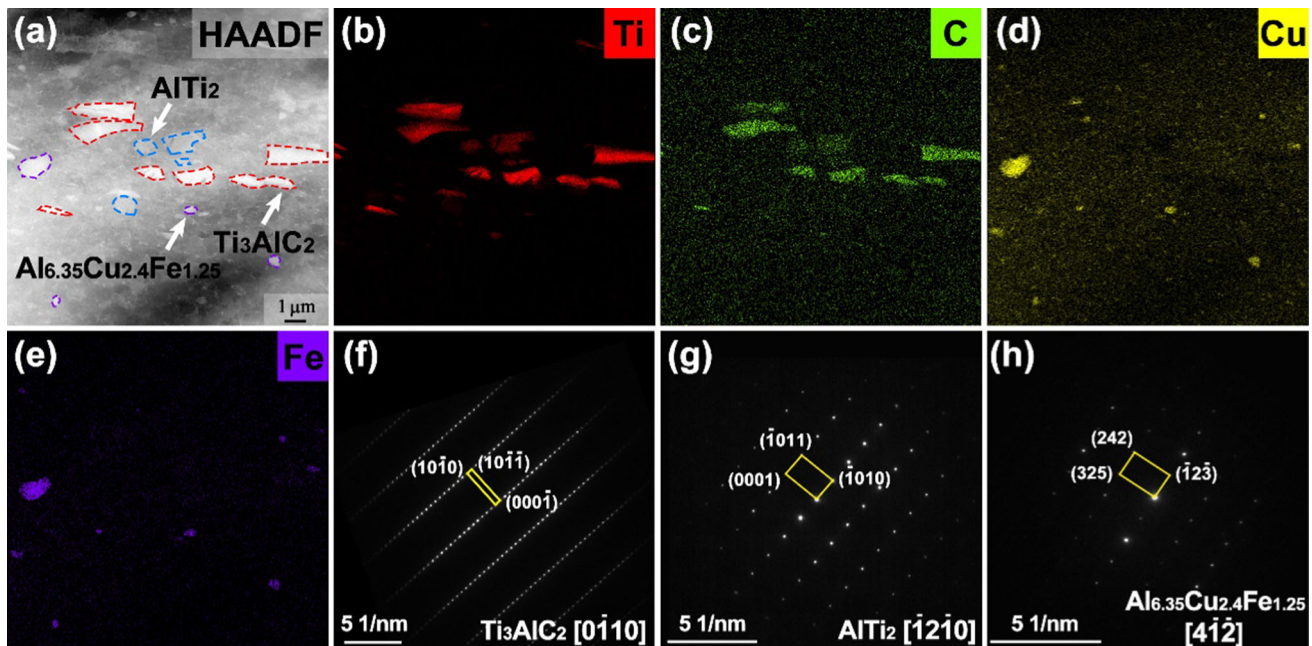


Figure 5 HAADF-STEM image (a) and corresponding EDS maps of Ti (b), C (c), Cu (d) and Fe (e) of the 2.25 vol.% Ti_3AlC_2 /2009Al composite. The SAED pattern of Ti_3AlC_2 (f), AlTi_2 (g), $\text{Al}_{6.35}\text{Cu}_{2.4}\text{Fe}_{1.25}$ (h).

and the fringes of Ti_3AlC_2 are still visible as shown in Fig. 6b. Further, the Ti_3AlC_2 -Al interface bonded well and was free from any other phase, which was beneficial to the load transfer strengthening. Figure 6c shows the inverse FFT image of the enlarged view responded to the white dotted rectangle in

Fig. 6b, numerous misfit regions (high density of dislocations and strained lattice) were observed at the interface and inside the grain of Ti_3AlC_2 and Al, which should be the geometrically necessary dislocation (GNDs). The GNDs formed due to the uncoordinated deformation between Al and ceramic

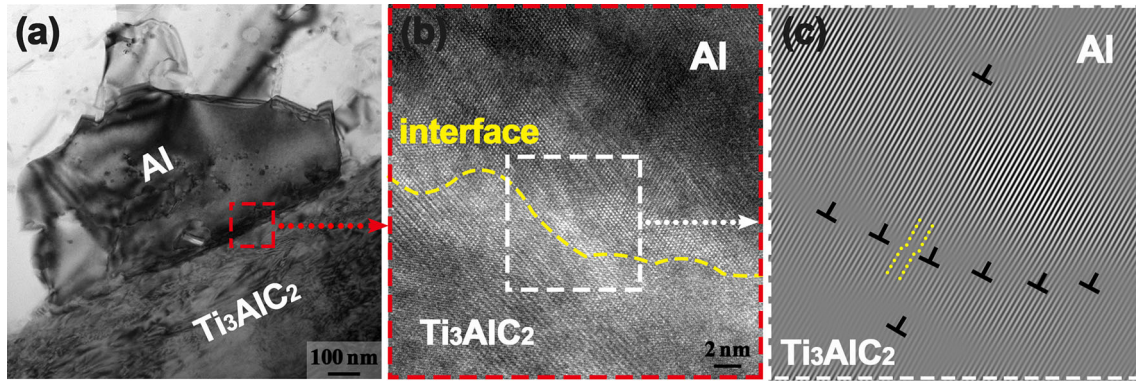


Figure 6 Bright-field TEM image of the 2.25 vol.% $Ti_3AlC_2/2009Al$ composite (a) and the HRTEM image of Ti_3AlC_2-Al interface (b), c inverse FFT image of the enlarged view responded to the white dotted rectangle in b. Misfit dislocation is marked as

‘L’ (For interpretation of the references to color in this figure legend, the reader is referred to the Web version of this article.)

particles, because they had significant difference in their elastic modulus and coefficient of thermal expansion [40, 41]. The dislocation strengthening provided by GNDs can be calculated by the following formula [17]:

$$\tau = \tau_0 + \alpha Gb\sqrt{\rho} \tag{1}$$

where the α is a constant, G is the shear modulus of matrix, b is the burgers vector, τ is the flow stress which is applied to dislocations, and ρ is the density of dislocation.

Mechanical properties

The mechanical properties of $Ti_3AlC_2/2009Al$ composites with different Ti_3AlC_2 concentrations are presented in Table 1 and Fig. 7a. The results indicated that the yield strength (YS) and ultimate tensile strength (UTS) increased nearly 45 MPa and 35 MPa, respectively, with an tiny sacrifice of elongation (El) of 1.5%, by introducing only 1.5 vol.% Ti_3AlC_2 . Further, it is difficult to achieve such high of UTS and YS for other ceramic reinforced particles (SiC, B_4C , Al_2O_3 , TiB_2 et al.) in the same particle content [3, 42]. The YS and UTS kept increasing with increasing the Ti_3AlC_2 concentration to 2.25 vol.%, but both of the

YS and UTS decreased as the Ti_3AlC_2 concentration increased to 3 vol.%. The reinforcements of Ti_3AlC_2 are supposed to be responsible for the load which could effectively transfer from matrix to reinforcement in order to enhance the strength of matrix. The load transfer effect from the reinforcement could be evaluated using the shear lag model, which could be described as the following formula [17]:

$$\sigma_{cy} = \sigma_{my} [V_p(S + 4)/4 + V_m] \tag{2}$$

where σ_{cy} and σ_{my} are the YS of the composites and matrix, respectively; the V_p and V_m are the volume fraction of reinforcement particle and Al matrix; S is the aspect ratio of reinforcement. The elastic modulus (E) of the $Ti_3AlC_2/2009Al$ composites was also increased due to the high modulus of Ti_3AlC_2 , and it could be effectively predicted by the rule of mixtures. The elastic modulus of 3 vol.% $Ti_3AlC_2/2009Al$ composite reached to 85 GPa, which was much higher than that of 2009Al alloy (77 GPa).

An interesting phenomenon was that, as the reinforcement concentration reaching 3 vol.%, the modulus of the composites increased; however, the strength of the composites began to decreased. This could attribute to the large Ti_3AlC_2 particle fracture during tension. As known, the modulus testing was

Table 1 Mechanical properties of $Ti_3AlC_2/2009Al$ composites with different Ti_3AlC_2 concentrations

| Sample | E (GPa) | YS (MPa) | UTS (MPa) | El (%) |
|--------------------------------|---------|----------|-----------|------------|
| 2009Al | 77 ± 1 | 567 ± 4 | 648 ± 7 | 12.3 ± 0.4 |
| 1.5 vol.% $Ti_3AlTi_2/2009Al$ | 81 ± 1 | 612 ± 2 | 681 ± 8 | 10.8 ± 0.5 |
| 2.25 vol.% $Ti_3AlTi_2/2009Al$ | 83 ± 1 | 625 ± 7 | 688 ± 11 | 8.6 ± 0.6 |
| 3 vol.% $Ti_3AlTi_2/2009Al$ | 85 ± 1 | 607 ± 2 | 683 ± 12 | 6.2 ± 0.5 |

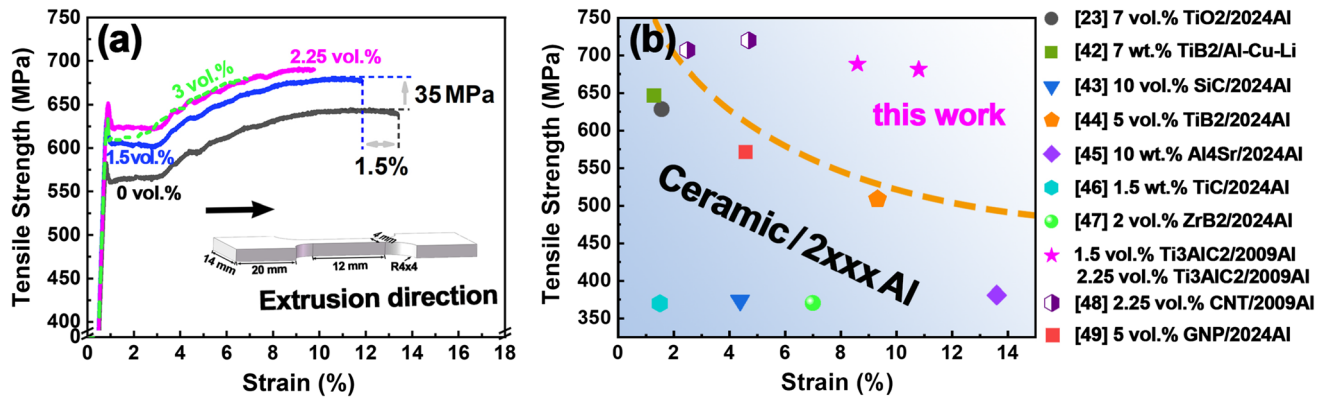


Figure 7 a Tensile stress–strain curves of Ti₃AlC₂/2009Al composites with different Ti₃AlC₂ concentrations; b a comparison of strength and ductility of the Ti₃AlC₂/2009Al

composites in present work with other works of ceramic reinforced 2xxx Al matrix composites [23, 43–50].

in the range of elastic deformation, which had a relatively lower stress level. However, the strength test had a much higher stress level, and thus the large Ti₃AlC₂ particle might fracture during strength test rather than modulus test.

The strength–ductility of different ceramics reinforced 2xxxAl composites is shown in Fig. 7b. It can be seen that Ti₃AlC₂/2009Al composites fabricated by HEBM achieved the highest strength while the plasticity was still high, as compared with ceramic particles (TiO₂, TiB₂, SiC, ZrB₂, TiC, Al₄Sr and TiB₂) and graphene nanoplatelets reinforced 2xxxAl composites. On the other hand, the EI of Ti₃AlC₂/2009Al composites is nearly three times of the carbon nanotube reinforced 2009Al composite, while their UTS were similar under the same fabrication method of HEBM. Apparently, the Ti₃AlC₂ with higher strength and sufficient deformability played a significant effect on the strengthening of Ti₃AlC₂/2009Al composites [15, 23].

The fracture surfaces of Ti₃AlC₂/2009Al composites with different Ti₃AlC₂ concentrations are shown in Fig. 8. It can be seen that a large number of micro-cracks and Al₂Cu phase (Fig. 8a–d) scattered over the fracture surface of the 2009Al matrix alloy. The secondary micro-cracks and Al₂Cu phase significantly reduced with the incorporation of 2.25 vol.% Ti₃AlC₂ (Fig. 8e, f). Further, scarcely any secondary micro-cracks and Al₂Cu phase could be found on the fracture surfaces as the Ti₃AlC₂ concentration increased to 3 vol.% (Fig. 8i–l).

The failure mechanism of Ti₃AlC₂/2009Al composites with different Ti₃AlC₂ concentrations can be schematically summarized in Fig. 9. The secondary

micro-cracks and Al₂Cu phase significantly reduced on the fracture surface with increasing the Ti₃AlC₂ concentration, which indicated that the fracture mostly occur at the site of Ti₃AlC₂, extraction and delamination were the dominant failure modes for Ti₃AlC₂ particles. However, for the 3 vol.% Ti₃AlC₂/2009Al composite, the existed cracks in larger Ti₃AlC₂ particles (Fig. 4h) would accelerate the failure during the tensile test.

In general, Ti₃AlC₂ extraction and delamination were the dominated deformation forms, which would effectively facilitate the compatible deformation between the reinforcement and metal matrix [15, 16]. The introduction of Ti₃AlC₂ could intact and bridge the crack faces in the wake of a growing crack. In this case, the crack tip was shielded by the deformation of ductile ligaments [10, 11, 39], which guaranteed Ti₃AlC₂/2009Al composites a relatively high plasticity as shown in Fig. 7b.

However, both of the YS and UTS decreased as Ti₃AlC₂ concentration increased to 3 vol.%. As shown in Fig. 4g, h, the size of Ti₃AlC₂ in 3 vol.% Ti₃AlC₂/2009Al composite was much larger than 1.5 vol.% and 2.25 vol.% Ti₃AlC₂/2009Al composites. Usually, large particles were more prone to fracture during extrusion process and tensile testing, which inhibited the load transfer effect from matrix to reinforcements [20]. In this way, the strength and ductility of Ti₃AlC₂/2009Al composites got worse. Further, the number of cracks in the large Ti₃AlC₂ particles for the 3 vol.% Ti₃AlC₂/2009Al composite was greater than the 2.25 vol.% Ti₃AlC₂/2009Al composite. The more cracks in Ti₃AlC₂ would cause materials failure easier

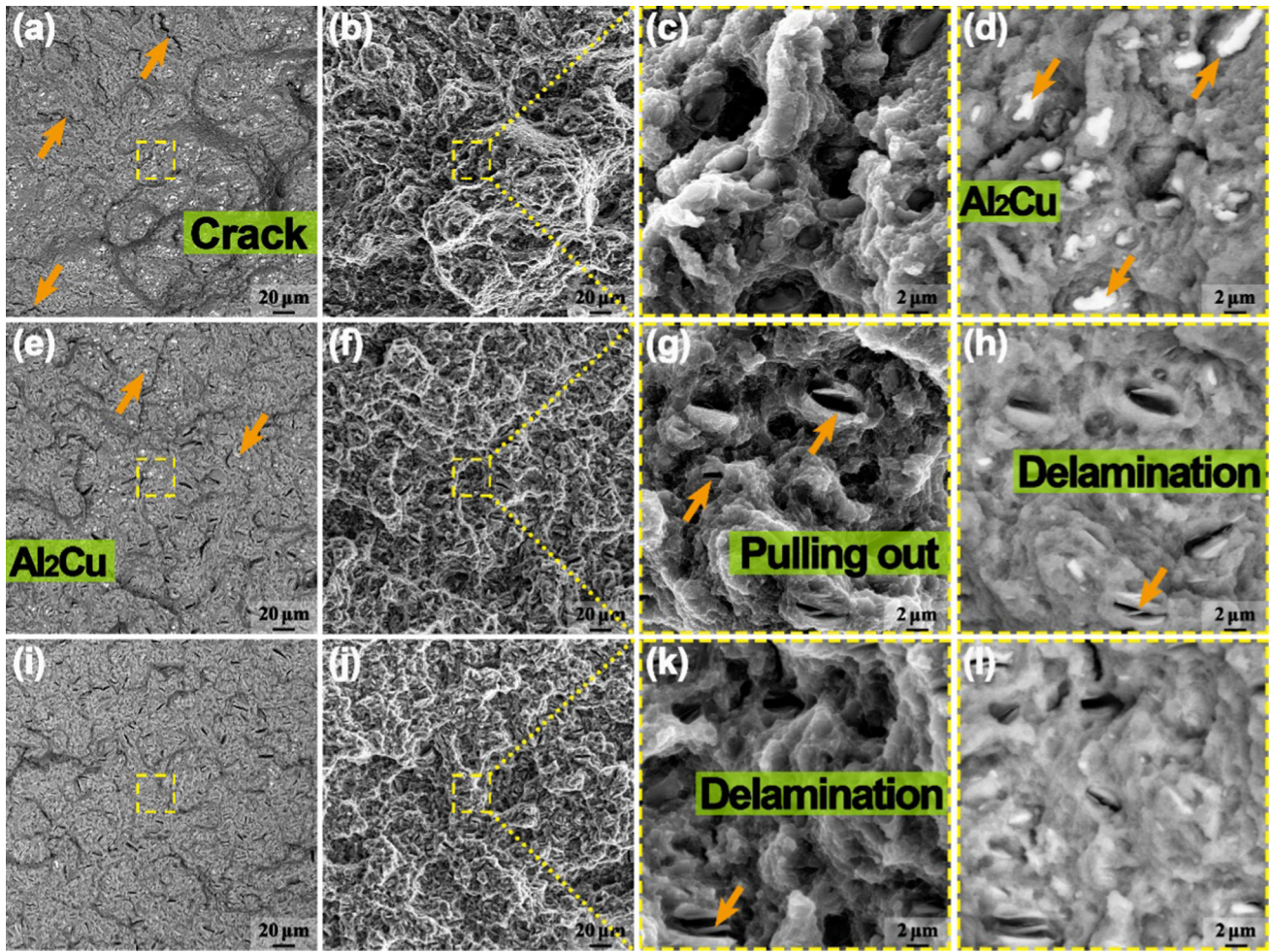


Figure 8 Fracture surfaces of $Ti_3AlC_2/2009Al$ composites with different Ti_3AlC_2 concentrations: a–d 0 vol.%, e–h 2.25 vol.%, i–l 3 vol.%; secondary electron SEM images b, c 0 vol.%, f, g 2.25 vol.%, j, k 3 vol.%.

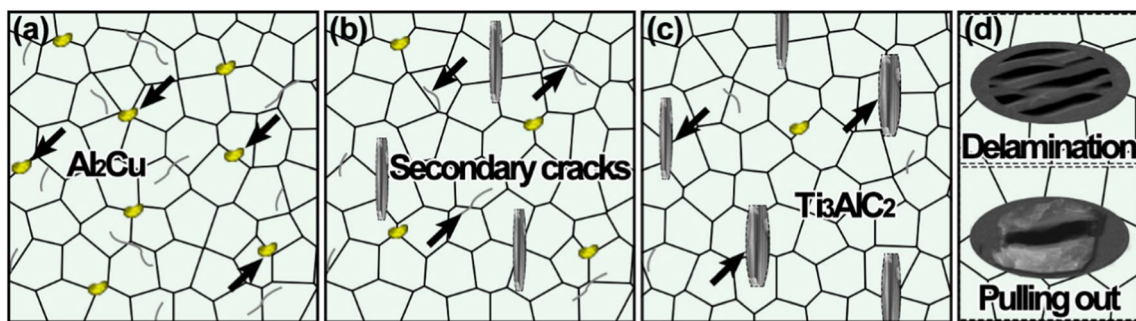


Figure 9 Schematic illustration of fracture behavior of $Ti_3AlC_2/2009Al$ composites with different Ti_3AlC_2 concentrations: a 0 vol.%, b 2.25 vol.% and c 3 vol.%; d the failure modes of Ti_3AlC_2 .

during tensile test, and this was another reason for the poor strength and ductility.

Conclusion

In this work, the Ti_3AlC_2 reinforced 2009Al composites were prepared successfully through HEBM technology combined with PM. The microstructure

and tensile properties of $\text{Ti}_3\text{AlC}_2/2009\text{Al}$ composites were explored. Some results could be concluded as follows:

- (1) Ti_3AlC_2 particles in 1.5 vol.% and 2.25 vol.% $\text{Ti}_3\text{AlC}_2/2009\text{Al}$ composites were significantly refined by HEBM, while Ti_3AlC_2 in 3 vol.% $\text{Ti}_3\text{AlC}_2/2009\text{Al}$ composite kept a relative larger size and cracks could be observed in some large Ti_3AlC_2 particles.
- (2) Most of the $\text{Ti}_3\text{AlC}_2\text{-Al}$ interface free from any other phase. The reaction products were strictly controlled, and only a few and fine reaction phase such as AlTi_2 was detected in $\text{Ti}_3\text{AlC}_2/2009\text{Al}$ composites.
- (3) The incorporation of 1.5 and 2.25 vol.% Ti_3AlC_2 kept the $\text{Ti}_3\text{AlC}_2/2009\text{Al}$ composite a high strength level of 680 MPa and a high modulus level of > 80 GPa. Ti_3AlC_2 extraction and delamination effectively facilitate the compatible deformation between reinforcement and metal matrix, providing the $\text{Ti}_3\text{AlC}_2/2009\text{Al}$ composite a high elongation of 10% and 8.6%.
- (4) The YS and UTS decreased as the Ti_3AlC_2 concentration increased to 3 vol.%, for the larger Ti_3AlC_2 particle size and the generation of cracks in larger Ti_3AlC_2 during the preparation process.

Acknowledgements

This work was supported by: (a) National Key R and D Program of China (Grant No. 2021YFA1600704); (b) National Natural Science Foundation of China (Nos. 52120105001, 52192594, 52192595, 51931009, 51871215, 51871214); (c) the Liaoning Excellent Youth Fund (No. 2022-YQ-01); (d) Shenyang young and middle-aged scientific and technological innovation talents support plan (No. RC210490); (e) the Youth Innovation Promotion Association CAS (No. 2020197).

Declarations

Conflict of interest The authors declare that they have no known competing financial interests or personal relationships that could have appeared to influence the work reported in this paper.

References

- [1] Liu ZY, Xiao BL, Wang WG, Ma ZY (2014) Tensile strength and electrical conductivity of carbon nanotube reinforced aluminum matrix composites fabricated by powder metallurgy combined with friction stir processing. *J Mater Sci Technol* 30:649–655
- [2] Xiao BL, Huang ZY, Ma K, Zhang XX, Ma ZY (2019) Research on hot deformation behaviors of discontinuously reinforced aluminum composites. *Acta Metall Sin* 55:59–72
- [3] Jawalkar CS, Verma AS, Suri NM (2017) Fabrication of aluminium metal matrix composites with particulate reinforcement: a review. *Mater Today Proc* 4:2927–2936
- [4] Liu ZY, Wang QZ, Xiao BL, Ma ZY, Liu Y (2010) Experimental and modeling investigation on SiCp distribution in powder metallurgy processed SiCp/2024 Al composites. *Mater Sci Eng A* 527:5582–5591
- [5] Zhu SZ, Wang D, Zan YN, Xiao BL, Ma ZY (2021) High strength SiCp/Al–2Cu–1.2Mg–0.6Si composite with weak natural aging hardening. *Compos Commun* 25:100742
- [6] Zhu SZ, Wang D, Xiao BL, Ma ZY (2021) Suppressed negative effects of natural aging by pre-aging in SiCp/6092Al composites. *Compos B Eng* 212:108730
- [7] Zan YN, Zhou YT, Liu ZY, Wang QZ, Wang WG, Wang D, Xiao BL, Ma ZY (2020) Microstructure and mechanical properties of $(\text{B}_4\text{C} + \text{Al}_2\text{O}_3)/\text{Al}$ composites designed for neutron absorbing materials with both structural and functional usages. *Mater Sci Eng A* 773:138840
- [8] Zan YN, Zhou YT, Liu ZY, Ma GN, Wang D, Wang QZ, Wang WG, Xiao BL, Ma ZY (2019) Enhancing strength and ductility synergy through heterogeneous structure design in nanoscale Al_2O_3 particulate reinforced Al composites. *Mater Des* 166:107629
- [9] Lü L, Lai MO, Su Y, Teo HL, Feng CF (2001) In situ TiB_2 reinforced Al alloy composites. *Scr Mater* 45:1017–1023
- [10] Peng LM, Wang JH, Li H, Zhao JH, He LH (2005) Synthesis and microstructural characterization of Ti– Al_3Ti metal–intermetallic laminate (MIL) composites. *Scr Mater* 52:243–248
- [11] Tom Scaria C, Pugazhenthir R (2021) Effect of process parameter on synthesizing of TiC reinforced Al7075 aluminium alloy nano composites. *Mater Today Proc* 37:1978–1981
- [12] Agne MT, Radovic M, Bentzel GW, Barsoum MW (2016) Stability of V_2AlC with Al in 800–1000 °C temperature range and in situ synthesis of $\text{V}_2\text{AlC}/\text{Al}$ composites. *J Alloy Compd* 666:279–286
- [13] Wang WJ, Gauthier Brunet V, Bei GP, Laplanche G, Bonneville J, Joulain A, Dubois S (2011) Powder metallurgy

- processing and compressive properties of Ti_3AlC_2/Al composites. *Mater Sci Eng A* 530:168–173
- [14] Hanaor DAH, Hu L, Kan WH, Proust G, Foley M, Karaman I, Radovic M (2016) Compressive performance and crack propagation in Al alloy/ Ti_2AlC composites. *Mater Sci Eng A* 672:247–256
- [15] Hu W, Huang Z, Wang Y, Li X, Zhai H, Zhou Y, Chen L (2021) Layered ternary MAX phases and their MX particulate derivative reinforced metal matrix composite: a review. *J Alloy Compd* 856:107629
- [16] Ghosh NC, Harimkar SP (2012) Consolidation and synthesis of MAX phases by spark plasma sintering (SPS): a review. *Advances in science and technology of Mn+1AX_n phases*. Elsevier, Amsterdam, p 47–80
- [17] Sun Y, Zhou C, Zhao Z, Yu Z, Wang Z, Liu H, Zhang N, Yang W, Wu G (2020) Microstructure and mechanical properties of Ti_2AlC particle and in-situ $TiAl_3$ reinforced pure Al composites. *Mater Sci Eng A* 785:139310
- [18] Hu L, O’Neil M, Erturun V, Benitez R, Proust G, Karaman I, Radovic M (2016) High-performance metal/carbide composites with far-from-equilibrium compositions and controlled microstructures. *Sci Rep* 6:35523
- [19] Peng L (2007) Fabrication and properties of Ti_3AlC_2 particulates reinforced copper composites. *Scr Mater* 56:729–732
- [20] Wang Z, Song M, Sun C, He Y (2011) Effects of particle size and distribution on the mechanical properties of SiC reinforced Al–Cu alloy composites. *Mater Sci Eng A* 528:1131–1137
- [21] Li J, Zhang X, Geng L (2018) Improving graphene distribution and mechanical properties of GNP/Al composites by cold drawing. *Mater Des* 144:159–168
- [22] Partoens B, Peeters FM (2006) From graphene to graphite: electronic structure around the *K* point. *Phys Rev B* 74:075404
- [23] Ma K, Liu ZY, Liu K, Chen XG, Xiao BL, Ma ZY (2021) Structure optimization for improving the strength and ductility of heterogeneous carbon nanotube/Al–Cu–Mg composites. *Carbon* 178:190–201
- [24] Liu ZY, Xiao BL, Wang WG, Ma ZY (2012) Singly dispersed carbon nanotube/aluminum composites fabricated by powder metallurgy combined with friction stir processing. *Carbon* 50:1843–1852
- [25] Ma K, Liu ZY, Bi S, Zhang XX, Xiao BL, Ma ZY (2021) Microstructure evolution and hot deformation behavior of carbon nanotube reinforced 2009Al composite with bimodal grain structure. *J Mater Sci Technol* 70:73–82
- [26] Ma K, Liu ZY, Liu BS, Xiao BL, Ma ZY (2021) Improving ductility of bimodal carbon nanotube/2009Al composites by optimizing coarse grain microstructure via hot extrusion. *Compos A Appl Sci Manuf* 140:106198
- [27] Zhang ZL, Zhai HX, Zhou Y, Huang ZY, Ai MX (2008) Preparation of composites from Al and Ti_3AlC_2 and its tribochemistry reactions against low carbon steel. *Key Eng Mater* 368–372:989–991
- [28] Manochehrian A, Heidarpour A, Mazaheri Y, Ghasemi S (2019) On the surface reinforcing of A356 aluminum alloy by nanolayered Ti_3AlC_2 MAX phase via friction stir processing. *Surf Coat Technol* 377:124884
- [29] Madhu HC, Edachery V, Lijesh KP, Perugu CS, Kailas SV (2020) Fabrication of wear-resistant Ti_3AlC_2/Al_3Ti hybrid aluminum composites by friction stir processing. *Metall Mater Trans A* 51:4086–4099
- [30] Nelson M, Agne MT, Anasori B, Yang J, Barsoum MW (2017) Synthesis and characterization of the mechanical properties of Ti_3SiC_2/Mg and Cr_2AlC/Mg alloy composites. *Mater Sci Eng A* 705:182–188
- [31] Wang Z, Ma Y, Sun K, Zhang Q, Zhou C, Shao P, Xiu Z, Wu G (2022) Enhanced ductility of Ti_3AlC_2 particles reinforced pure aluminum composites by interface control. *Mater Sci Eng A* 832:142393
- [32] Sun Y, Zhao Z, Wu G (2022) Microstructure characterization and mechanical properties of in situ synthesized $Ti_2(Al, Si)C$ reinforced Al composites. *Mater Charact* 191:112176
- [33] Li XN, Liu ZY, Dai ZX, Feng H, Xiao BY, Ni DR, Wang QZ, Wang D, Ma ZY (2022) Wear behavior of the uniformly dispersed carbon nanotube reinforced 6061Al composite fabricated by milling combined with powder metallurgy. *Acta Metall Sin (Engl Lett)* 35:1765–1776
- [34] Li XN, Liu ZY, Zan YN, Xiao BL, Ni DR, Wang QZ, Wang D, Ma ZY (2021) Wear behavior of the raw and pre-smashed carbon nanotubes reinforced 6061Al composites fabricated by powder metallurgy. *Sci China Technol Sci* 65:1149–1159
- [35] Liu ZY, Ma K, Fan GH, Zhao K, Zhang JF, Xiao BL, Ma ZY (2020) Enhancement of the strength–ductility relationship for carbon nanotube/Al–Cu–Mg nanocomposites by material parameter optimisation. *Carbon* 157:602–613
- [36] Gonzalez-Julian J (2020) Processing of MAX phases: from synthesis to applications. *J Am Ceram Soc* 104:659–690
- [37] Medkour Y, Roumili A, Maouche D, Louail L (2012) Electrical properties of MAX phases. *Advances in science and technology of Mn+1AX_n phases*. Elsevier, Amsterdam, p 159–175
- [38] von Treinfeldt JE, Firestein KL, Fernando JFS, Zhang C, Siriwardena DP, Lewis CEM, Golberg DV (2021) The effect of Ti_3AlC_2 MAX phase synthetic history on the structure and electrochemical properties of resultant Ti_3C_2 MXenes. *Mater Des* 199:109403

- [39] Chao ZL, Zhang LC, Jiang LT, Qiao J, Xu ZG, Chi HT, Wu GH (2019) Design, microstructure and high temperature properties of in-situ Al_3Ti and nano- Al_2O_3 reinforced 2024Al matrix composites from Al-TiO₂ system. *J Alloy Compd* 775:290–297
- [40] Tariq NH, Gyansah L, Qiu X, Du H, Wang JQ, Feng B, Yan DS, Xiong TY (2018) Thermo-mechanical post-treatment: a strategic approach to improve microstructure and mechanical properties of cold spray additively manufactured composites. *Mater Des* 156:287–299
- [41] Zan YN, Zhang Q, Zhou YT, Liu ZY, Wang QZ, Wang D, Xiao BL, Ren WC, Ma ZY (2020) Introducing graphene (reduced graphene oxide) into Al matrix composites for enhanced high-temperature strength. *Compos B Eng* 195:108095
- [42] Ramnath BV, Elanchezian C, Annamalai RM, Aravind S, Atreya TSA, Vignesh V, Subramanian C (2014) Aluminium metal matrix composites—a review. *Rev Adv Mater Sci* 38:55–60
- [43] Zheng Z, Zhang X, Qian M, Li J, Imran M, Geng L (2022) Ultra-high strength GNP/2024Al composite via thermomechanical treatment. *J Mater Sci Technol* 108:164–172
- [44] Shin JH, Choi HJ, Bae DH (2024) The structure and properties of aluminum composites reinforced with TiO₂ nanoparticles. *Mater Sci Eng A* 607(2014):605–610
- [45] Emamy M, Oliayee M, Tavighi K (2015) Microstructures and tensile properties of Al/2024–Al₄Sr composite after hot extrusion and T6 heat treatment. *Mater Sci Eng A* 625:303–310
- [46] Su J, Li Y, Duan MG, Liu S, Liu K (2018) Investigation on particle strengthening effect in in-situ TiB₂/2024 composite by nanoindentation test. *Mater Sci Eng A* 727:29–37
- [47] Yang H, Tian S, Gao T, Nie J, You Z, Liu G, Wang H, Liu X (2019) High-temperature mechanical properties of 2024Al matrix nanocomposite reinforced by TiC network architecture. *Mater Sci Eng A* 763:138121
- [48] Zhang ZY, Chen G, Zhang SL, Zhao YT, Yang R, Liu MP (2019) Enhanced strength and ductility in ZrB₂/2024Al nanocomposite with a quasi-network architecture. *J Alloy Compd* 778:833–838
- [49] Zhao B, Yang Q, Wu L, Li X, Wang M, Wang H (2019) Effects of nanosized particles on microstructure and mechanical properties of an aged in-situ TiB₂/Al–Cu–Li composite. *Mater Sci Eng A* 742:573–583
- [50] Li PB, Chen TJ, Qin H (2016) Effects of mold temperature on the microstructure and tensile properties of SiCp/2024 Al-based composites fabricated via powder thixoforming. *Mater Des* 112:34–45

Publisher's Note Springer Nature remains neutral with regard to jurisdictional claims in published maps and institutional affiliations.

Springer Nature or its licensor (e.g. a society or other partner) holds exclusive rights to this article under a publishing agreement with the author(s) or other rightsholder(s); author self-archiving of the accepted manuscript version of this article is solely governed by the terms of such publishing agreement and applicable law.